buildings

MDPI

Article

Characterization of the Mechanical Properties of Fiber-Reinforced Modified High Water Content Materials

Bao Song [1], Jinxing Lyu [1,2], Zhiyi Zhang [1,*], Zhimeng Song [1] and Songxiang Liu [1]

[1] School of Geology and Mining Engineering, Xinjiang University, Urumqi 830046, China; 107552404741@stu.xju.edu.cn (B.S.); lvjinxing@xju.edu.cn (J.L.); 107552304862@stu.xju.edu.cn (Z.S.); lsx8856528@stu.xju.edu.cn (S.L.)
[2] School of Mining Engineering, China University of Mining and Technology, Xuzhou 221116, China
* Correspondence: xjuzhiyi@163.com

Abstract

This research examines the mechanical properties of fiber-reinforced modified high-water content materials intended for mining backfill applications. Conventional high-water content materials encounter several challenges, including brittleness, inadequate crack resistance, and insufficient later-stage strength. Basalt fiber (BF) and polypropylene fiber (PP) were integrated into the material system to establish a reinforcing network through interfacial bonding and bridging mechanisms to mitigate these issues. A total of nine specimen groups were developed to assess the influence of fiber type (BF/PP), fiber content (ranging from 0.5% to 2.0%), and water cement ratio (from 1.25 to 1.75) on compressive, tensile, and shear strengths. The findings indicated that basalt fiber exhibited superior performance compared to polypropylene fiber, with a 1% BF admixture yielding the highest compressive strength of 5.08 MPa and notable tensile enhancement attributed to effective pore-filling and three-dimensional reinforcement. Conversely, higher ratios (e.g., 1.75) resulted in diminished strength due to increased porosity, while a ratio of 1.25 effectively balanced matrix integrity and fiber reinforcement. Improvements in shear strength were less significant, as excessive fiber content disrupted interfacial friction, leading to a propensity for brittle failure. In conclusion, basalt fiber-modified high water content materials (with a 1% admixture and a ratio of 1.25) demonstrate enhanced ductility and mechanical performance, rendering them suitable for mining backfill applications. Future investigations should focus on optimizing the fiber matrix interface, exploring hybrid fiber systems, and conducting field-scale validations to promote sustainable mining practices.

Keywords: fiber-reinforced high water materials; basalt fiber; polypropylene fiber; ratio; mechanical properties; compressive strength; tensile strength; shear strength

check for updates

Academic Editor: Rajai Zuheir Al-Rousan

Received: 28 May 2025
Revised: 25 June 2025
Accepted: 26 June 2025
Published: 28 June 2025

Citation: Song, B.; Lyu, J.; Zhang, Z.; Song, Z.; Liu, S. Characterization of the Mechanical Properties of Fiber-Reinforced Modified High Water Content Materials. *Buildings* **2025**, *15*, 2283. https://doi.org/10.3390/buildings15132283

Copyright: © 2025 by the authors. Licensee MDPI, Basel, Switzerland. This article is an open access article distributed under the terms and conditions of the Creative Commons Attribution (CC BY) license (https://creativecommons.org/licenses/by/4.0/).

1. Introduction

Following extensive, high-intensity, and large-scale mining operations [1], the availability of coal resources characterized by favorable burial conditions and high quality in the central and western regions of China has been steadily declining. Concurrently [2,3], there is an increasing demand for deep mining and resource extraction in the context of complex geological conditions [4,5]. In response to these challenges, high-water material-filling mining technology has emerged as a significant solution [6,7]. Currently, the most commonly utilized high-water materials consist of sulfoaluminate cement clinker or silicate cement combined with additives (such as suspension agents and retarders) designated as the A

material, and quicklime, gypsum, among others, supplemented with additional additives (such as suspension agents and rapid setting early strength agents) classified as the B material [8]. These components are mixed with water separately to create a two-component mixture, which can achieve a rapid initial setting and attain a specific strength within a short timeframe [8,9]. Nevertheless, high-water materials exhibit limitations, including high brittleness, inadequate crack resistance, and insufficient strength in practical applications [10–13]. Consequently, optimizing their physical and mechanical properties has become a critical concern for ensuring mine safety and promoting efficient production [13]. Presently, research focused on the incorporation of modified high-water materials has emerged as a pivotal area for the application and advancement of these materials, although much of the existing work primarily emphasizes the utilization of related industrial solid waste [14].

Fiber reinforcement technology has emerged as a significant method for enhancing material properties and has found extensive applications across various sectors, including construction, transportation, and water conservancy [15]. Recent investigations by numerous experts and scholars have focused on the sustainable utilization of fibers. For instance, Wang et al. [16] examined the synergistic effects of fiber reinforcement and microbial-induced carbonate precipitation (MICP) stabilization on the tensile properties of oolitic sand. Their findings indicate that the integration of fiber reinforcement with MICP technology markedly enhances the tensile behavior of oolitic sand, with fiber content and length playing crucial roles in determining tensile properties. This research offers novel insights and methodologies for the stabilization of coastal engineering projects. Similarly, Song et al. [17] explored the mechanisms underlying the synergistic reinforcement of polypropylene (PP) composites through the incorporation of basalt fibers (BFs) and cellulose nanocrystals (CNCs). Their study revealed that CNCs enhance the crystallinity of PP via heterogeneous nucleation and establish hydrogen bonding interactions with BF, thereby inhibiting the movement of PP molecular chains. The combined effects of these materials significantly bolster the mechanical properties of the composite. Zhang et al. [18,19] investigated the mechanical properties of fiber-reinforced polymer composites at extremely low temperatures (−170 °C) and observed notable improvements in compressive and flexural strengths. However, this enhancement was accompanied by increased brittleness and reduced ductility. Their research indicated that steel fibers were more effective than polypropylene fibers in mitigating the adverse effects of low temperatures on material brittleness.

This article aims to examine research pertaining to fiber-modified high-water materials utilizing fiber reinforcement technology. The underlying principle involves the formation of composite materials by integrating high-strength and high-modulus fiber materials with matrix substances. The reinforcement of fiber-modified high-water materials is primarily reflected in the enhancement of mechanical properties [20], the suppression of crack propagation, and the improvement of durability. Basalt fiber (BF), derived from natural basalt, is a low-carbon and abundant synthetic fiber material, with global reserves exceeding one trillion tons [21,22]. Its environmental benefits are evident throughout its lifecycle, as it requires no chemical beneficiation during extraction, and the melt-drawing process generates no wastewater or exhaust emissions. The energy consumption associated with its production is only one-fifth that of carbon fiber [23]. Polypropylene fiber (PP), produced from polypropylene resin sourced mainly from recycled plastics such as masks and packaging materials, exemplifies the transformation of waste plastics into engineering materials, characterized by low cost and lightweight properties [24–27]. The incorporation of these two synthetic fiber materials into high-water material systems is anticipated to mitigate the performance limitations of high-water materials, thereby enhancing their

physical and mechanical properties and improving their engineering applicability. Despite some scholarly work on doped-modified high-water materials, comprehensive studies addressing the physical and mechanical properties of fiber-modified high-water materials remain relatively limited [28], particularly concerning the effects of variables such as fiber content and ratio on the mechanical properties of these modified materials.

In light of the aforementioned context, this article investigates various types of fiber-modified high-water materials as the primary subject of research. The study involves the direct incorporation of fibers into high-water materials, resulting in the formation of a uniformly dispersed reinforcement network through mechanical mixing and physical modification. A series of mechanical performance assessments, including tests for compressive, shear, and tensile strength, are conducted to examine the effects of different fiber types, fiber content, and ratios on the physical and mechanical properties of the modified materials, as well as to elucidate the fiber reinforcement mechanisms at play. The objective of this research is to provide a theoretical foundation and technical support for the scientific application of fiber-modified high-water materials in mine-filling engineering, thereby fostering innovative advancements in mine-filling technology and contributing to the safe and environmentally sustainable extraction of mineral resources [29].

2. Experimental Program

2.1. Test Sample Design

A total of nine groups of specimens were prepared for this investigation, with the design principle of the specimens grounded in the analysis and comparison of the mechanical properties of materials subjected to various combinations of fiber doping and high water material ratios. The detailed design and categorization of the specimens are presented in Table 1. Each group comprises three samples that maintain identical ratios. Series 1 serves as the control group, wherein the only variable is the ratio, with fiber doping set at 0%. Series 2 constitutes the experimental group, with samples differentiated by the ratio of the high-water material, the type of fiber utilized, and the fiber admixture. The test samples are designated according to a specific nomenclature. In this system, "BF" denotes basalt fibers, "PP" indicates polypropylene fibers, the first numeral represents the ratio of the high-water material, the second numeral signifies the fiber admixture, and the final numeral is a Roman numeral indicating samples with the same zone ratio design. For instance, the designation BF-1.50-1.0-II refers to the second test sample within the group characterized by a ratio of 1.5 and a basalt fiber admixture of 1%.

Table 1. Design of experimental programs.

Series	Groups	Samples	Ratio (W/C)	Fiber Types	Fiber Admixture (in %)
Series 1	H-1.25-0.0	H-1.25-0.0%-I, II, III	1.25	-	0
	H-1.50-0.0	H-1.50-0.0%-I, II, III	1.5	-	0
	H-1.75-0.0	H-1.75-0.0%-I, II, III	1.75	-	0
Series 2	BF-1.25-1.0	BF-1.25-1.0%-I, II, III	1.25	basalt fiber	1%
	BF-1.50-1.0	BF-1.50-1.0%-I, II, III	1.5	basalt fiber	1%
	BF-1.75-1.0	BF-1.75-1%-I, II, III	1.75	basalt fiber	1%
	BF-1.25-0.5	BF-1.25-0.5%-I, II, III	1.25	basalt fiber	0.5%
	BF-1.25-2.0	BF-1.25-2.0%-I, II, III	1.25	basalt fiber	2%
	PP-1.25-1.0	PP-1.25-1.0%-I, II, III	1.25	polypropylene fiber	1%

This study employs the MTS pressure testing system to perform mechanical strength assessments on samples, as illustrated in Figure 1. In the uniaxial compressive strength evaluation, strain gauges (SGs) are affixed to the specimen's surface in a configuration comprising one horizontal and one vertical gauge per group, totaling three groups, to facilitate the measurement of axial and circumferential strains. The modified high-water material exhibits inherently low tensile properties, with its tensile strength typically ranging from one-tenth to one-half of its compressive strength. The integration of fibers with the modified high-water material creates a reinforcement network through interfacial bonding, which accommodates a portion of the tensile stress during tension and mitigates crack propagation. The bonding characteristics at the fiber matrix interface are critical to the material's shear strength, as the fibers distribute shear stress via a bridging mechanism, thereby inhibiting crack advancement. Consequently, shear tests were also conducted. By the "Standard for Testing the Mechanical Properties of Ordinary Concrete," a displacement loading mode was employed for all sample tests, with a displacement loading rate established at 1.0 mm/min.

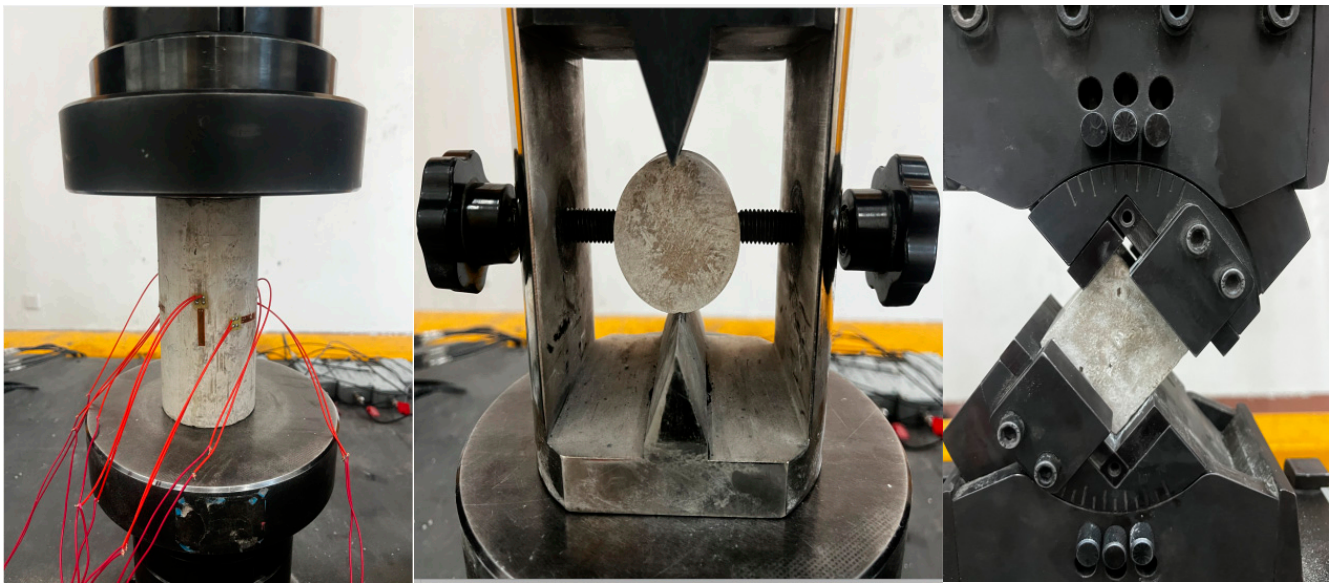

(**A**) (**B**) (**C**)

Figure 1. Test setup: (**A**) strain gauge arrangement; (**B**) Brazilian split test; (**C**) shear test.

2.2. Raw Materials

High water backfill material is supplied by Hebei Guangkai Building Material Technology Co., Ltd. based in Shijiazhuang, China. This material comprises two main components, referred to as Part A and Part B. Part A is primarily composed of aluminum sulfate cement, a suspending agent, and a coagulation retarder, while Part B consists of a mixture of lime, gypsum, a suspending agent, and an early-strengthening agent. The basalt fiber and polypropylene fiber utilized in the study were produced and supplied by Weifang Zhongxin Material Technology Co., Ltd. (Weifang, China), demonstrating a compressive strength of 374 MPa and a density of 0.91 g/cm^3.

2.3. Specimen Preparation

The procedure for preparing fiber-modified high-water material samples is illustrated in Figure 2. Initially, the mass of each raw material is precisely measured by the predetermined ratio. Subsequently, water is added for mixing; high water material A and material B are placed in separate containers, and water is evenly distributed into the mixing bucket. The mixture is stirred for five minutes, after which the pre-weighed fibers are incorporated into the slurry of materials A and B and thoroughly mixed. Following this, the mixture is shaped into molds and allowed to cure for 24 h before demolding. By the national standard for the testing of mechanical properties of ordinary concrete (GB/T 50081) [30], the prepared samples are covered with a protective film and placed in a curing chamber maintained at a temperature of 20 ± 2 °C and relative humidity of at least 95%. Mechanical testing is conducted after a curing period of seven days.

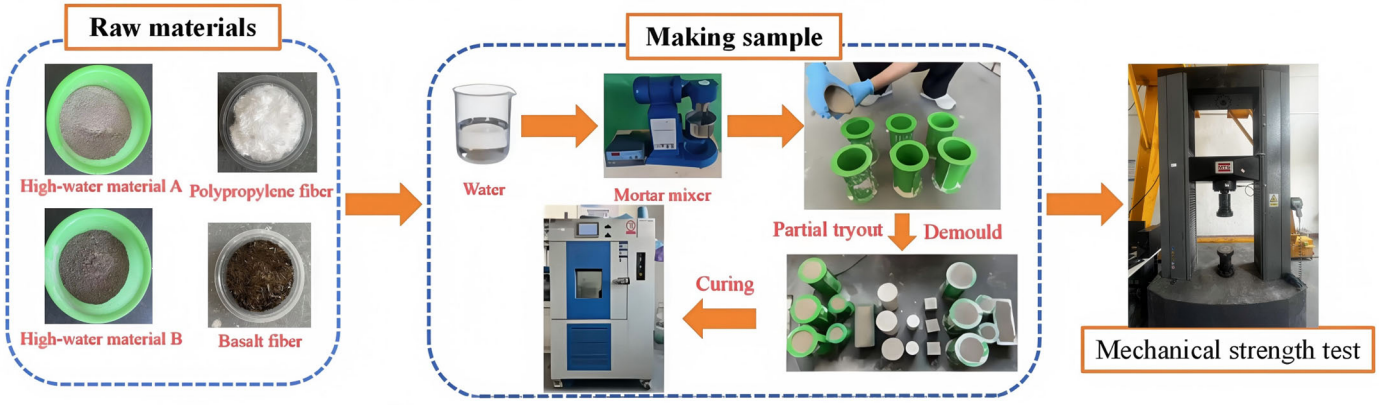

Figure 2. The flow of specimen preparation for modified high water materials.

3. Experimental Results and Discussion

3.1. Stress Strain Curve

Using the MTS pressure testing system, the stress strain curves for each sample were obtained, as shown in Figure 3.

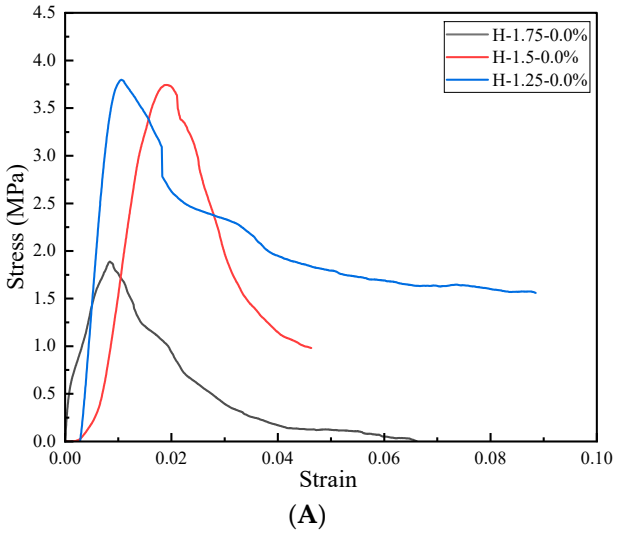

(**A**)

Figure 3. *Cont.*

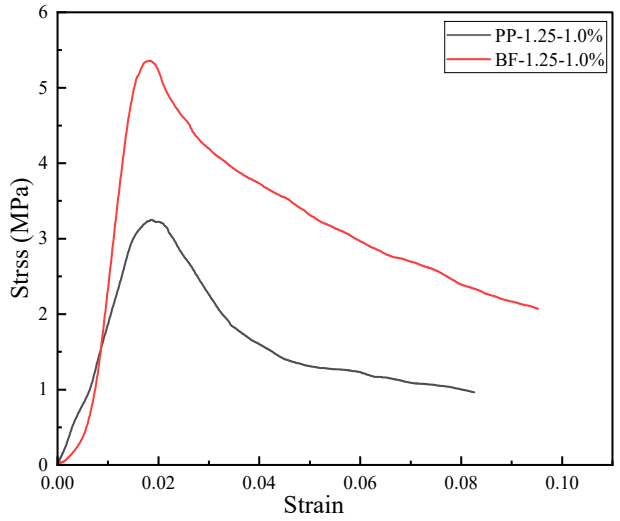

(**B**)

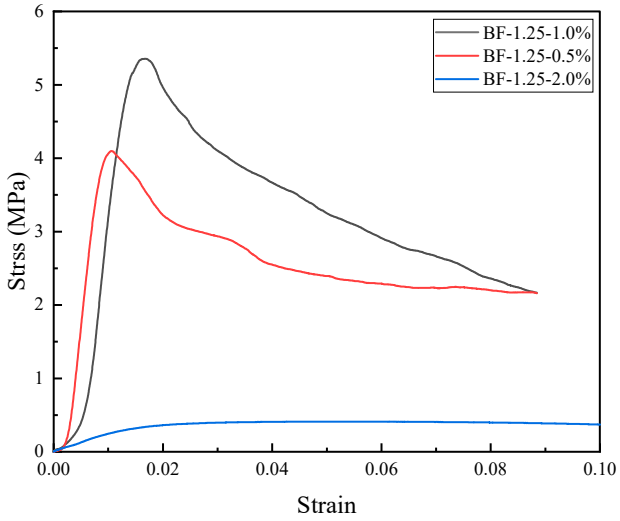

(**C**)

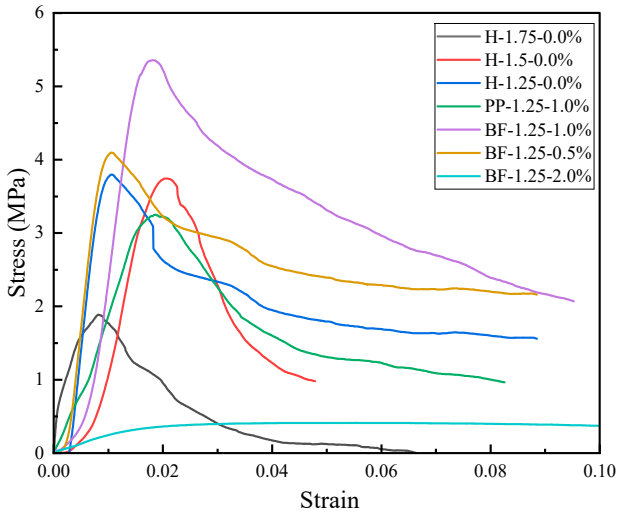

(**D**)

Figure 3. Stress strain curves of the specimens of modified high-water materials: (**A**) with 0% fiber doping and three different ratios (1.25, 1.50, and 1.75), (**B**) with a ratio of 1.25 and two different fibers, BF (1%) and PP (1%), and (**C**) with a ratio of 1.25 and three different basaltic fiber dopings (0.5%, 1%, and 2%). (**D**) Overall stress strain diagram.

As illustrated in Figure 3A–D, the incorporation of fibers significantly alters the characteristics of the stress strain curves for modified high-water materials. These curves encompass four distinct stages: pore compaction, elastic deformation, yielding, and damage. However, the modified high-water materials display differing characteristics across these stages when compared to pure high-water materials.

In the pore compression stage, pure high-water materials (e.g., H-1.25-0%, H-1.5-0%, and H-1.75-0%) exhibit a more pronounced pore compression, which intensifies with an increasing ratio (see Figure 3A). Conversely, for fiber-modified high-water materials, the dedaoyixianeircharacteristic curves become less distinct as fiber content increases (refer to Figure 3B,C). The pore structure within pure high-water materials remains consistent, with variations in pore size and quantity corresponding to different ratios. During the initial loading phase, the compression of pores results in a reduction of the material's volume, leading to elevated initial stress levels. The presence of fibers may result in a more gradual increase in stress during the pore-compaction stage, potentially yielding higher stress values due to the dispersive effect of the fibers, which enhances the material's initial stiffness.

In the elastic deformation phase, pure high-water materials (Figure 3A) and those with low fiber content (Figure 3C) exhibit a less pronounced but prolonged elastic deformation phase. This is attributed to the bridging effect of the fibers, which mitigates the propagation of microcracks and may slightly extend the linear range of the elastic phase. However, as fiber content increases, this phase becomes less pronounced (Figure 3C,D). This phenomenon is particularly evident in the modified materials BF-1.25-2%, where uneven fiber dispersion results in localized areas of excessively high or low fiber density, thereby diminishing the overall uniform reinforcement effect and leading to lower peak stress.

During the yield stage, specimens display a distinct rupture surface, with the rupture process continuing to evolve. Increased fiber content allows the fibers to share part of the load, resulting in an increase in yield stress with higher fiber doping levels. Notably, at a fiber doping level of 1%, the effect is significant, while at 2% (Figure 3C), the ductility of the fibers contributes to a more gradual development of strain in the plastic phase, characterized by minor fluctuations in the curve as the fibers progressively fracture or are pulled out.

In the destruction phase, fiber-modified high-water materials demonstrate distinct characteristics. The stress strain curves indicate a more pronounced decline for the pure high-water material (see Figure 3A). Conversely, the material with a ratio of 1.25 exhibits a flatter curve, and its elevated residual strength may be attributed to its porosity and the relatively weak cementation structure. The stress strain curves for other pure high-water materials also exhibit a steeper decline (refer to Figure 3A). In comparison to the pure high-water materials, an increase in fiber content correlates with higher residual strength at maximum strain. Specifically, specimens containing 2% basalt fibers display a more gradual performance compared to those with 1% fibers. This improvement is likely due to the formation of a denser three-dimensional network by the additional fibers, which effectively restricts crack propagation and postpones the onset of strain softening.

Utilizing the stress strain data presented in Figure 3, we employed a trilinear segmentation approach to evaluate each specimen. Based on Table 2, we can obtain the following analysis content.

Table 2. Trilinear Modulus Analysis Table.

Sample Number	E1 (GPa)	E2 (GPa)	E3 (GPa)	E2/E1 Ratio	Peak Intensity (MPa)
H-1.25-0.0%	0.86–1.00	2.42–2.68	0.31–0.47	2.7–2.8	4.10
H-1.50-0.0%	0.72–0.84	2.18–2.42	0.28–0.38	2.9–3.0	3.74
H-1.75-0.0%	0.46–0.56	1.32–1.52	0.16–0.26	2.8–3.2	1.89
BF-1.25-1.0%	1.18–1.32	3.15–3.45	0.62–0.78	2.6–2.7	5.36
BF-1.25-0.5%	0.86–1.00	2.42–2.68	0.31–0.47	2.7–2.8	4.10
BF-1.25-2.0%	0.68–0.82	1.92–2.18	0.22–0.35	2.7–2.9	3.20
PP-1.25-1.0%	0.72–0.86	1.95–2.22	0.25–0.38	2.6–2.7	3.25

E1 Stage (Initial Compaction Modulus): During the initial loading phase (0–20% of peak stress), the presence of fibers enhances the material's initial stiffness by effectively occupying the pores. As the ratio increases from 1.25 to 1.75, the E1 value decreases from 1.00 GPa to 0.56 GPa, representing a reduction of 44%. The fiber content significantly influences E1, with a value of 1.00 GPa observed at 0.5% fiber content, peaking at 1.32 GPa at 1.0% (a 32% increase compared to the control group), and subsequently declining to 0.82 GPa at 2.0% due to fiber aggregation. The E1 value plays a crucial role in the deformation control capacity of the filling material under initial loading conditions and is a vital parameter for ensuring the early stability of mine filling materials.

E2 Stage (Elastic Modulus): The E2 value indicates the stiffness characteristics during the primary load-bearing phase of the material. The incorporation of basalt fiber significantly enhances E2 from 2.68 GPa to 3.45 GPa (an increase of 29%), whereas polypropylene fiber exhibits a limited effect, achieving only 2.22 GPa. The ratio demonstrates a pronounced sensitivity to E2; as it rise from 1.25 to 1.75, E2 experiences a substantial decline from 2.68 GPa to 1.52 GPa. E2 influences both the deformation characteristics and the load-bearing capacity of the filling material.

E3 Stage (Post-Peak Modulus): E3 represents the residual load-bearing and toughness characteristics of the material following failure. The E3 value for BF-1.25-1.0% reaches 0.78 GPa, which is 166% of the control group, indicating exceptional toughness. The ratio significantly affects E3, which decreases from 0.47 GPa to 0.26 GPa (a reduction of 45%), with notable differences observed among fiber types. The E3 value for basalt fiber is 106% greater than that of polypropylene fiber. As a critical indicator of the ductility failure characteristics of the material, E3 is essential for ensuring mine safety and long-term stability.

E2/E1 Ratio Analysis: The E2/E1 ratio serves as an indicator of the transition characteristics of materials from the compaction phase to the elastic stage. The E2/E1 ratio for BF-1.25-1.0% is recorded at 2.6–2.7, suggesting a favorable transition between stages. Conversely, the material with a ratio of 1.75 exhibits a higher E2/E1 ratio (up to 3.2), indicating an excessively prolonged initial compaction stage.

3.2. Uniaxial Compressive Strength Test of Specimen

The compressive strength of the specimen is generally taken as the stress value at the peak point of the stress strain curve, which can be calculated according to the following formula:

$$P = F/A \quad (1)$$

where: P is compressive strength, MPa; F is the axial loading load, kN; A for the specimen cross-sectional area, mm^2.

The combined proportioning design of fiber-modified high water material compressive strength is illustrated in Figure 4, where the fiber dosage is maintained at 1%. It is observed that as the ratio of the material increases, the compressive strength of the specimens exhibits a decreasing trend. Specifically, at a ratio of 1.25, the compressive strength decreases from a maximum of 5.08 MPa to 3.15 MPa. When basalt and polypropylene fibers are incorporated into the material at a ratio of 1.25, it is noted that the modified samples containing basalt fiber demonstrate a higher uniaxial compressive strength, averaging 1.21 MPa more than those containing polypropylene fiber.

The study further investigates the optimal ratio and the type of fiber added, focusing on the impact of basalt fiber dosage on the compressive strength of the modified samples. As the basalt fiber content increases from a low to a high level of 2%, the compressive strength of the modified samples initially increases and then decreases, reaching a peak strength of 5.08 MPa at a 1% dosage. This phenomenon can be attributed to the ability of a lower dosage of basalt fibers to effectively fill the pores within the material, thereby enhancing its strength during the initial phase. However, as the reaction period progresses, the limited space for pore filling restricts the regeneration of calcium aluminate, resulting in minimal changes in strength. Conversely, an excessive amount of basalt fiber leads to partial pore filling and the formation of a weak internal structure, as well as the creation of new pores, ultimately causing a reduction in the material's strength.

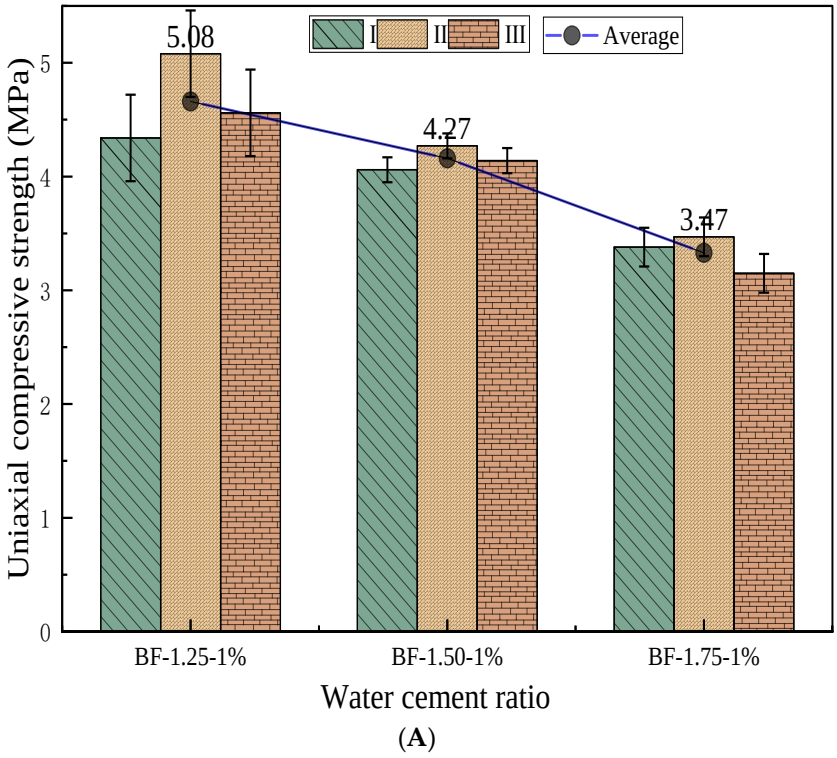

Figure 4. *Cont.*

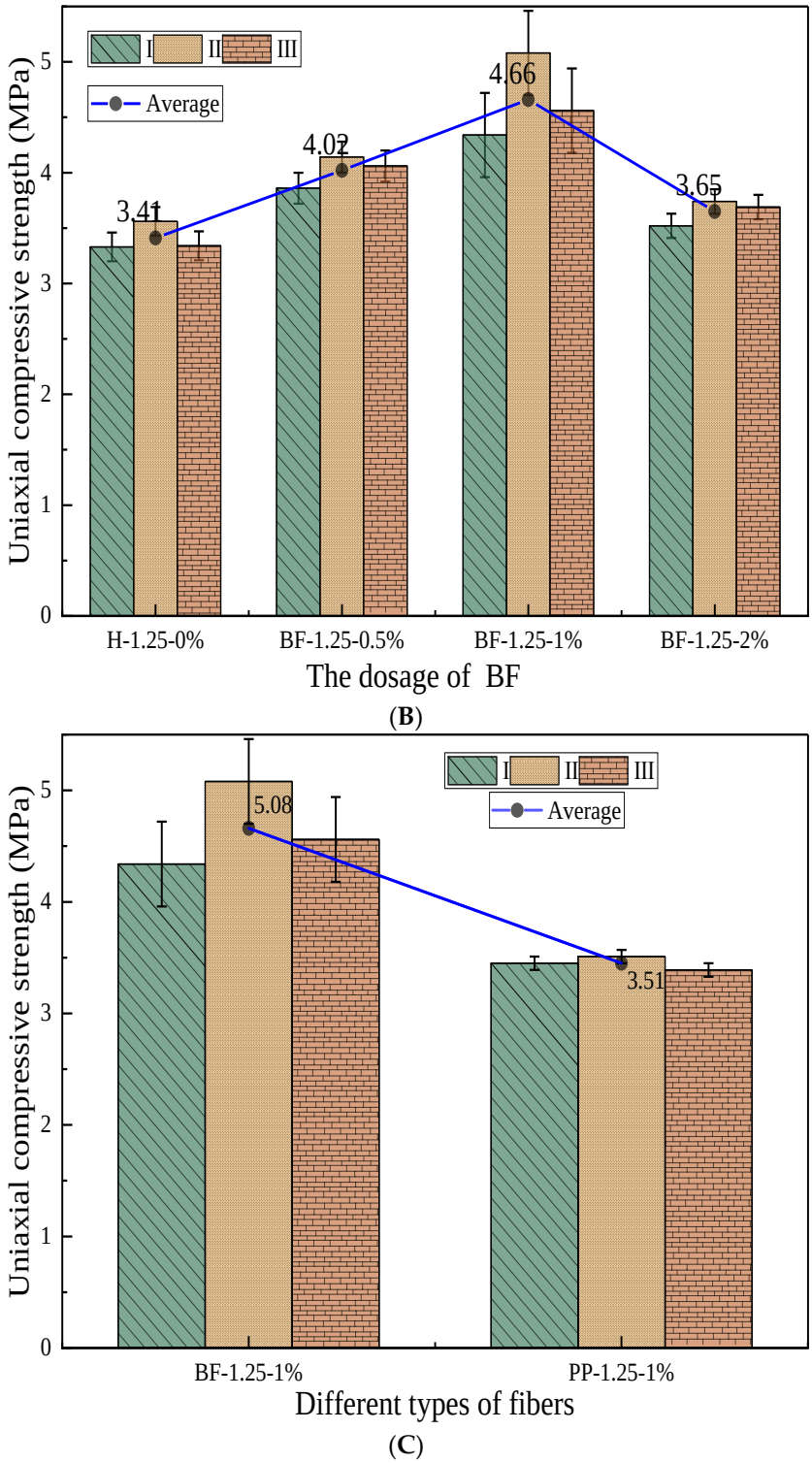

Figure 4. Uniaxial compressive strength plots: (**A**) with 1% fiber incorporation and three different ratios (1.25, 1.50, 1.75), (**B**) with a ratio determined to be 1.25 for medium and high water materials and with four different basalt fiber incorporations (0%, 0.5%, 1%, and 2%) (**C**) with a ratio of 1.25 and with two different fibers BF (1%) and PP (1%).

3.3. Tensile Strength Test

In the Brazilian split test, three specimens were prepared for each group, varying in high water material ratios, fiber dosages, and fiber types. The tensile strength was

subsequently calculated by the equation, following the exclusion of the maximum and minimum values of the peak load.

$$\sigma_t = \frac{2P_{max}}{\pi dL} \quad (2)$$

where: σ_t is the tensile strength, MPa; P_{max} is the peak load size, N; d is the diameter of the cylindrical specimen, mm; L is the height of the specimen, mm.

The Brazilian split line graph illustrates significant fluctuations in overall tensile strength, revealing that the tensile strength of fiber-reinforced materials surpasses that of non-reinforced counterparts. This observation underscores the role of fiber in enhancing the tensile properties of the material. An increase in the ratio correlates with a decrease in tensile strength, attributed to the heightened porosity that diminishes the bonding capacity. When the modified high-water material exhibits a ratio of 1.25, the incorporation of 0.5%, 1%, and 2% basalt fiber yields a relative peak at 1%. The insufficient dispersion of 0.5% fiber results in weak interfacial bonding, while the agglomeration of 2% fiber induces localized stress concentrations, thereby reducing the enhancement efficiency. Conversely, the addition of 1% fiber facilitates the formation of a continuous three-dimensional network, where chemical bonding predominates the enhancement mechanism, complemented by the lapping effect associated with fiber network formation. The combination of a 1.25 ratio with 1% fiber is deemed suitable for applications such as filling in open pit mine end gangs and deep mining hollow areas. The tensile strength anomalies observed with the 2% basalt fiber suggest that both excessive and insufficient fiber doping can adversely affect tensile strength. Notably, the enhancement efficiency of basalt fiber exceeds that of polypropylene fibers, particularly at dosages greater than 1%. The ratio of 1.25 represents a critical threshold that balances matrix strength and fiber reinforcement, making it the optimal choice for this application.

Figure 5 Tensile strength graphs: three sets of tensile strength values averaged for three different ratios (1.25, 1.50, 1.75), different fiber dosages (0%, 0.5%, 1%, 2%), two different fibers, BF (1%) and PP (1%).

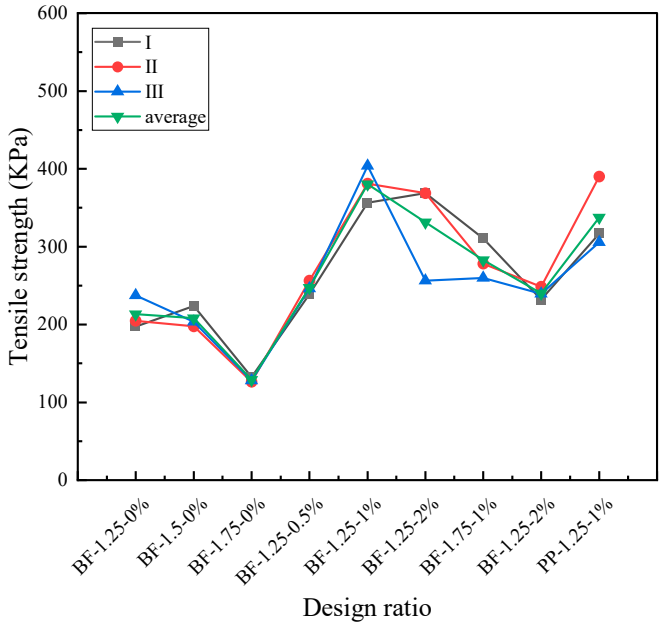

Figure 5. Tensile strength diagram.

3.4. Shear Strength Test

This experiment adopts the angle die shear test, choosing 45°, 50°, and 55° as the three angles of specifications for 50 mm cube specimens, shear surface normal stress, and shear stress were calculated according to the following formula:

$$\sigma = \frac{P}{A} \tag{3}$$

where: σ for the role of the normal stress on the shear surface, MPa; P for the role of the normal load on the shear surface, N; A for the effective shear surface area, mm^2; τ for the role of the shear stress on the shear surface, MPa; Q for the role of the shear load on the shear surface, N.

Plot the shear strength under different normal stresses σ in the τ-c coordinate system, and use the least squares method to fit and obtain the rock shear strength parameters:

$$\tau = \sigma \tan \psi + C \tag{4}$$

where: τ for the role of the shear strength, MPa; ψ for the role of the friction, C for the role of the cohesion, MPa.

Figure 6 illustrates that the shear strength of fiber-reinforced materials exhibits considerable variability, suggesting that such materials outperform their non-reinforced counterparts in terms of shear strength. A numerical trend analysis reveals that the shear strength of the control group, which lacks fiber reinforcement, fluctuates between 0.6 and 0.8 MPa. In contrast, the incorporation of basalt fibers results in a notable enhancement of shear strength, elevating it to a range of 0.8 to 1.4 MPa. Specifically, the BF-1.25-0.5% group achieved a maximum shear strength of 1.4 MPa, while the BF-1.25-1% and BF-1.25-2% groups recorded shear strengths of 1.2 MPa and 1.3 MPa, respectively, all of which surpass the values observed in the fiber-free combinations.

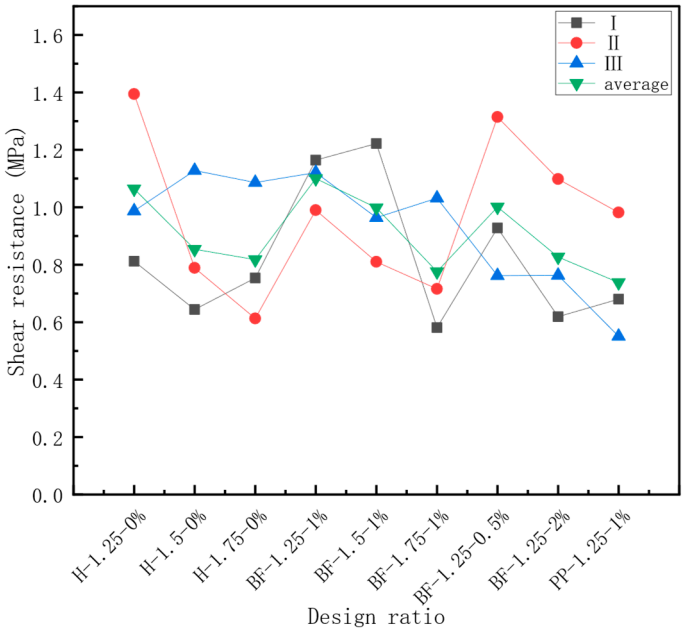

Figure 6. Shear strength diagram.

Furthermore, an increase in the ratio is significantly correlated with a reduction in shear strength, attributed to diminished bonding capacity resulting from increased porosity. For a fiber content of 1%, shear strength consistently decreases from 1.2 MPa at a ratio of 1.25 to 1.0 MPa at a ratio of 1.5,and further to 0.8 MPa at a ratio of 1.75. At a ratio of 1.25,

the addition of 0.5%, 1%, and 2% basalt fibers yields shear strengths of 1.4 MPa, 1.2 MPa, and 1.3 MPa, respectively, with the highest value observed at 0.5% fiber content.

Analysis of failure modes indicates that while a fiber content of 0.5% results in high shear strength, inadequate fiber dispersion leads to weak local interface bonding, culminating in brittle shear failure. Conversely, a fiber content of 2% results in fiber aggregation, which causes local stress concentrations and the formation of weak channels along the aggregated fibers, thereby diminishing reinforcement efficiency. The introduction of 1% fibers facilitates the development of a three-dimensional network, allowing the fibers to effectively traverse the shear plane during shear failure, thereby exhibiting ductile failure characteristics. The combination of a ratio of 1.25 and 1% fiber content is deemed suitable for applications such as filling open-pit mine end walls and deep mining hollow areas. The variability in shear strength values associated with 2% basalt fibers underscores the detrimental effects that both excessive and insufficient fiber incorporation can have on shear performance. Notably, the reinforcement efficiency of basalt fibers surpasses that of polypropylene fibers, particularly when the dosage exceeds 1%. The ratio of 1.25 is identified as a critical threshold for optimizing the balance between matrix strength and fiber reinforcement, rendering it the most favorable choice for this application. Figure 6 Shear strength graph: three sets of tensile strength values averaged for three different ratios (1.25, 1.50, 1.75), different fiber dosages (0%, 0.5%, 1%, 2%), and two different fibers, BF (1%) and PP (1%).

3.5. Material Performance Evaluation Based on Comparative Analysis

Following the established standards for mine filling materials, the compressive strength is typically mandated to be no less than 3.0 MPa, while the tensile strength must be at least 0.3 MPa. Experimental findings indicate that a compressive strength of 5.08 MPa, along with a corresponding tensile strength achieved through an optimal mixture of 1% basalt fiber and a ratio of 1.25, satisfies the engineering specifications. Conversely, a compressive strength of 3.15 MPa observed with a higher ratio (e.g., 1.75) is only marginally above the minimum requirement, suggesting a reduced safety margin.

Advantages of basalt fiber material include: (1) Exceptional interfacial bonding capabilities, as evidenced by scanning electron microscopy (SEM) analysis, which reveals a dense array of hydration products adhering to the fiber surface, thereby establishing a robust interfacial transition zone; (2) A notable enhancement effect, demonstrated by a compressive strength increase of 1.21 MPa compared to polypropylene fiber at a 1% dosage; (3) A well-defined three-dimensional network structure that effectively mitigates crack propagation.

Conversely, the limitations of basalt fiber material are as follows: (1) The optimal dosage range is limited, with performance deterioration observed due to fiber aggregation at a dosage of 2%; (2) The material is sensitive to the ratio, as the quality of interfacial bonding significantly diminishes when the ratio exceeds 1.25; (3) The enhancement in shear strength is constrained, with a maximum of 1.4 MPa at a 0.5% dosage, which is only marginally higher than the 1.2 MPa observed at a 1% dosage, suggesting that the mechanisms governing shear failure differ from those of tensile and compressive failure.

The optimal ratio exhibits favorable ductility characteristics while satisfying strength requirements, rendering it suitable for applications in mining filling engineering. Nonetheless, precise control over the accuracy of the ratio is essential to ensure performance stability. It is important to note that variations in mining filling materials arise from differing conditions, necessitating a detailed analysis of specific issues.

4. Micromorphological Analysis

To further investigate the bridging mechanism and the impact of fiber-induced three-dimensional network formation, we employed a German Zeiss Sigma 300 scanning electron microscope (SEM) to analyze the microstructure of fiber-modified high water materials with varying ratios. Figure 7 illustrates the dispersion and microstructural characteristics of fibers within high-water materials at a magnification of 10,000.

The SEM images reveal distinct dispersion and network formation states within the three-dimensional space. A comparative analysis of the microstructure of fibers at a 1% content across different ratios indicates that the interface between the fiber and the matrix is most closely bonded at a ratio of 1.25. At this ratio, a significant quantity of hydrated gel and ettringite crystals adheres to the fiber surface, resulting in a dense interface transition zone. Conversely, as the ratio increases to 1.50 and 1.75, a greater number of pores appear around the fibers, leading to a marked decline in the quality of interface bonding, with some fibers exhibiting debonding from the matrix.

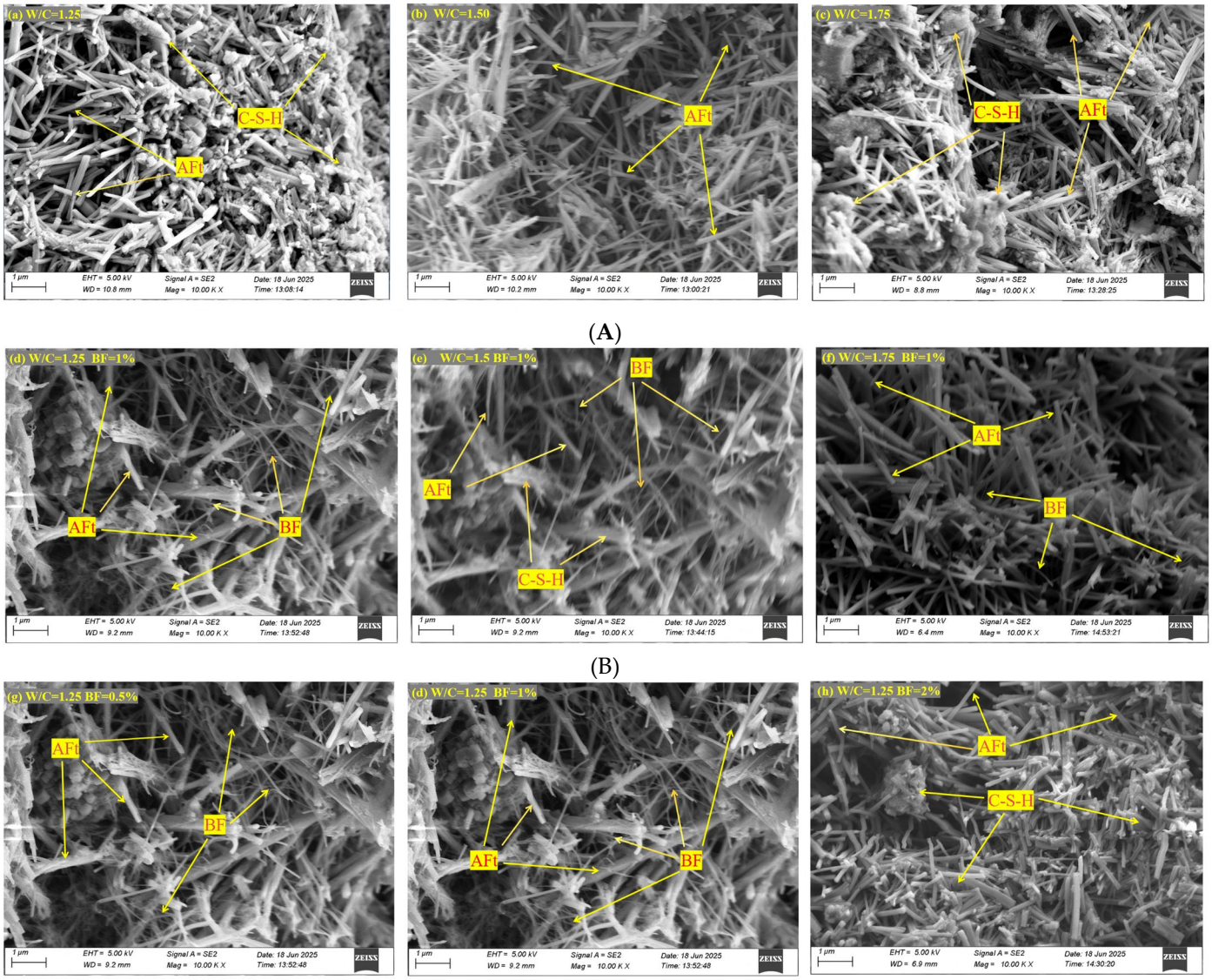

Figure 7. *Cont.*

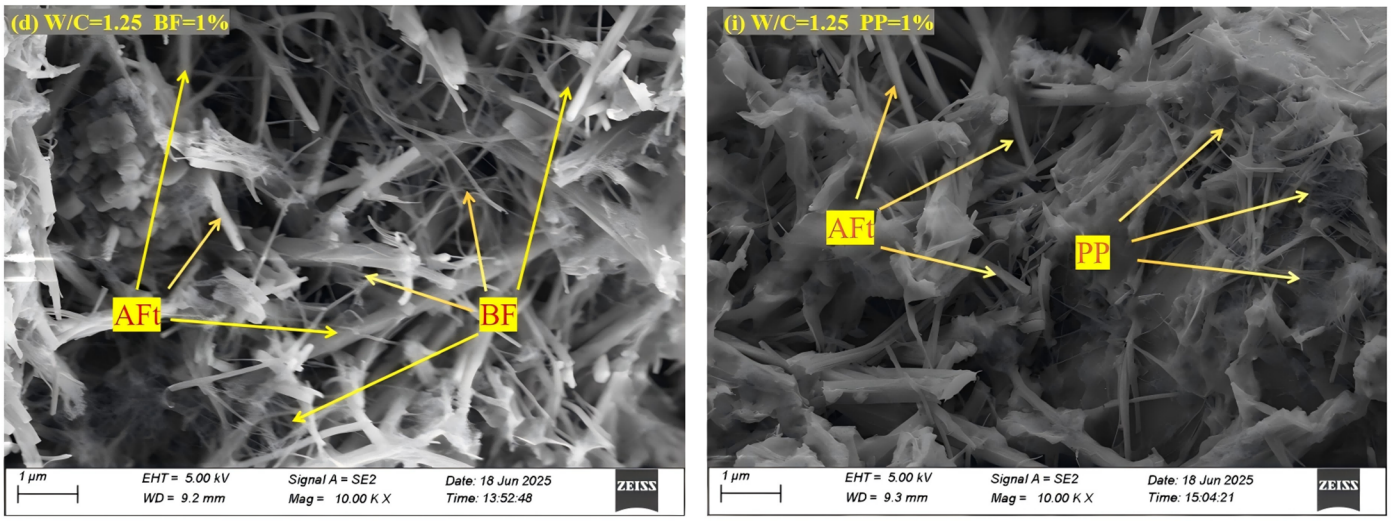

(**D**)

Figure 7. SEM images: (**A**) No fiber content and three different w/c ratios (1.25, 1.5, and 1.75); (**B**) BF = 1% and three different w/c ratios (1.25, 1.5, and 1.75). (**C**) w/c = 1.25 and three different Basalt fiber content (0.5%, 1.0%, and 2%). (**D**) When w/c = 1.25, BF = 1% and PP = 1%.

In the comparative analysis of fiber content, a 0.5% fiber content results in a relatively low fiber quantity. Although individual fibers demonstrate strong bonding with the matrix, the formation of an effective three-dimensional network structure is hindered, thereby limiting the bridging effect. At a dosage of 1%, the fibers are uniformly distributed within the matrix, and multiple fibers interlace to create a comprehensive spatial network, effectively bridging microcracks in the matrix and enhancing reinforcement. The surrounding matrix structure is dense, with a significant reduction in porosity. However, when the fiber content increases to 2%, localized fiber aggregation occurs, leading to the formation of weak interfaces between certain fiber bundles. Additionally, an excessive fiber quantity elevates the matrix porosity, thereby compromising the overall material performance.

Microstructural analysis of polypropylene fibers under identical conditions (1% dosage and 1.25 ratio) reveals a relatively uniform distribution; however, the interface bonding with the material matrix is weaker compared to that of basalt fibers. The quantity of hydration products adhering to the surface is lower, resulting in insufficient bonding density. This weak interface bonding adversely affects the bridging capability of the fibers, yielding a reinforcement effect that is inferior to that of basalt fibers.

The findings from the microstructural observations indicate that at a fiber content of 1% and a ratio of 1.25, basalt fibers can establish the optimal three-dimensional network structure within the matrix, characterized by superior interface bonding quality and an effective bridging mechanism. These results align with the outcomes of macroscopic mechanical performance tests.

5. Conclusions

This research conducted a systematic examination of the mechanical properties of fiber-reinforced modified high-water content materials through an extensive experimental analysis. The following conclusions can be drawn from the study:

(1) Identification of Optimal Configuration: The combination of 1% basalt fiber content with a ratio of 1.25 yielded the highest compressive strength of 5.08 MPa, establishing it as the optimal configuration for mining backfill applications. This configuration effectively balances the integrity of the matrix with the efficiency of fiber reinforcement.

(2) Comparison of Fiber Types: Basalt fiber exhibited superior performance relative to polypropylene fiber, with an average compressive strength that was 1.21 MPa higher. Scanning Electron Microscopy (SEM) analysis indicated that basalt fibers form stronger interfacial bonds with the matrix, characterized by dense hydration products adhering to the fiber surface, whereas polypropylene fibers displayed weaker interfacial bonding and inadequate bonding density.

(3) Effects of Ratio: An increase in the ratio from 1.25 to 1.75 led to a significant reduction in strength across all mechanical properties. Specifically, the compressive strength decreased from 5.08 MPa to 3.15 MPa, which can be attributed to increased porosity and a reduction in bonding capacity at higher ratios.

(4) Optimization of Fiber Content: A fiber dosage of 1% was determined to be optimal for all strength parameters. Lower dosages (0.5%) resulted in inadequate fiber dispersion and weak network formation, while higher dosages (2%) led to fiber aggregation, stress concentrations, and diminished reinforcement efficiency.

(5) Microstructural Validation: SEM analysis at a magnification of 10,000 confirmed the establishment of an effective three-dimensional fiber network under optimal conditions. The 6 mm basalt fibers demonstrated excellent dispersion, robust bonding with the matrix, and effective bridging mechanisms that inhibit crack propagation, thereby enhancing the overall performance of the material.

(6) Engineering Implications: The optimized basalt fiber-modified high-water material exhibits improved ductility and mechanical performance, making it suitable for mining backfill applications. It offers enhanced crack resistance and long-term stability compared to conventional high-water materials.

These findings provide a robust foundation for the practical application of fiber-reinforced high-water materials in mining engineering, contributing to safer and more sustainable mining operations. In light of the optimal ratio of 1% basalt fiber to a ratio of 1.25 established in this study, subsequent research endeavors should prioritize the enhancement of the fiber matrix interface bonding performance through the application of surface modification technologies, thereby augmenting reinforcement efficiency. Concurrently, investigations into the synergistic effects of combining basalt fiber with other fiber materials should be pursued to facilitate performance improvements. Additionally, it is imperative to conduct on-site engineering verification tests to assess the long-term performance and economic viability of the optimized ratio under actual mining filling conditions, thereby providing robust engineering data to support its promotion and application.

Author Contributions: J.L.: Writing—review & editing. Z.Z.: Writing—original draft. Z.S.: Writing—review & editing, Writing—original draft. B.S.: Writing—original draft. S.L.: Writing—original draft. All authors have read and agreed to the published version of the manuscript.

Funding: This study was financially supported by the Natural Science Foundation of the Key Research and Development of Xinjiang Uygur Autonomous Region, China (2023B01009-1).

Data Availability Statement: Data will be made available on request.

Conflicts of Interest: The authors declare no conflicts of interest.

References

1. Zhou, J.; Pan, J.; Xia, Y.; Du, T.; Liu, W.; Zhang, C. Mechanism and prevention of coal bursts in gob-side roadway floor under thick and hard roof in the deep mining area of Ordos. *Int. J. Coal Sci. Technol.* **2024**, *11*, 80. [CrossRef]
2. Xue, H.; Jiang, B.; He, M.; Zhang, C.; Wang, Y.; Zhang, S.; Deng, Y. Mechanism and validation of pressure relief and energy reduction of automatically formed roadway by roof cutting in deep coal mines. *Bull. Eng. Geol. Environ.* **2025**, *84*, 77. [CrossRef]

3. Zhao, W.; Zhao, D.; Wang, K.; Fan, L.; Zhao, Z.; Dong, H.; Shu, L. Will greenhouse gas emissions increase with mining depth in coal mines? An analysis of gas occurrence under varying in-situ stress conditions. *Sci. Total Environ.* **2024**, *945*, 173957. [CrossRef]
4. Xu, J.; Zhou, R.; Song, D.; Li, N.; Zhang, K.; Xi, D. Deformation and damage dynamic characteristics of coal-rock materials in deep coal mines. *Int. J. Damage Mech.* **2019**, *28*, 58–78. [CrossRef]
5. Bo, L.; Yang, S.; Liu, Y.; Wang, Y.; Zhang, Z. Research on the data validity of a coal mine solid backfill working face sensing system based on an improved transformer. *Sci. Rep.* **2023**, *13*, 11092. [CrossRef]
6. Lyu, J.; Song, Z.; Chen, H.; Qi, Z.; Yu, B.; Hu, H. Behavior of backfill material made of high-water material and recycled concrete lumps for highwall mining. *Case Stud. Constr. Mater.* **2024**, *21*, e03777. [CrossRef]
7. Xing, K.; Cheng, J.; Zhen, Z.; Wan, Z.; Han, Z.; Yan, W.; Lv, J.; Yang, Y. Effect of super-high water materials backfilling on stress decrease and energy release during strip coal pillar mining, A case study. *Heliyon* **2024**, *10*, e37441. [CrossRef]
8. Sun, Y.; Xie, S.; Wu, C.; Cui, J.; Chen, D.; Guo, F.; Jiang, Z.; Ren, Y.; Lu, W. Influence of the ultra-fine fly ash dosages on the mechanical properties of the sulfoaluminate cement-based high water backfilling material. *Sci. Rep.* **2023**, *13*, 1564. [CrossRef] [PubMed]
9. Gao, M.; Li, M.; Wang, J.; Yang, P.; Xu, M. Effect of fly ash on properties and hydration of calcium sulphoaluminate cement-based materials with high water content. *Rev. Adv. Mater. Sci.* **2024**, *63*, 20240046. [CrossRef]
10. Ma, X.; Liu, C.; Zhai, L.; Xie, S.; Wu, C.; Yang, J. Study on hydration mechanism and ratio optimization of slag powder modified high-water material. *Sci. Rep.* **2025**, *15*, 6175. [CrossRef]
11. Wu, H.K.; Liu, C.W.; Zhang, Z.; Miao, Y.C. Time effect of chloride erosion on physical and mechanical properties of high-water-content materials. *Adv. Mater. Sci. Eng.* **2020**, *2020*, 2730283. [CrossRef]
12. He, W.; Liu, L.; Fang, Z.; Gao, Y.; Sun, W. Effect of polypropylene fiber on properties of modified magnesium-coal-based solid waste backfill materials. *Constr. Build. Mater.* **2023**, *362*, 129695. [CrossRef]
13. Xie, S.; Sun, Y.; Wang, E.; Chen, D.; Wu, X.; Qi, P. Experimental and mechanistic research on modifying the mechanic properties of the high water backfill material by electrochemical treatment. *Sci. Rep.* **2020**, *10*, 17027. [CrossRef]
14. Ren, C.; Wang, W.; Yao, Y.; Wu, S.; Yao, X. Complementary use of industrial solid wastes to produce green materials and their role in CO_2 reduction. *J. Clean. Prod.* **2020**, *252*, 119840. [CrossRef]
15. Pang, Z.; Lu, C.; Liu, J.; Yao, Y.; Wang, J. Experimental study of tensile properties of strain-hardening cementitious composites (SHCCs) reinforced with innovative twisted basalt fibers. *Structures* **2023**, *48*, 1977–1988. [CrossRef]
16. Wang, D.L.; Tang, C.S.; Pan, X.H.; Liu, B.; Shi, B. Coupling effect of fiber reinforcement and MICP stabilization on the tensile behavior of calcareous sand. *Eng. Geol.* **2023**, *317*, 107090. [CrossRef]
17. Song, D.; Wang, B.; Tao, W.; Wang, X.; Zhang, W.; Dai, M.; Li, J.; Zhou, Z. Synergistic reinforcement mechanism of basalt fiber/cellulose nanocrystals/polypropylene composites. *Nanotechnol. Rev.* **2022**, *11*, 3020–3030. [CrossRef]
18. Zhang, H.; He, B.; Cheng, Y.; Tang, Y.; Ren, Q.; Zhu, X.; Jiang, Z. Strengthening and embrittlement effect of cryogenic temperature on fiber reinforced geopolymer composite. *Cem. Concr. Compos.* **2024**, *153*, 105727. [CrossRef]
19. Zhang, X.; Shi, X.; Li, X.; Ning, J.; Liu, Y.; Yang, S. Research and development of steel fiber reinforced concrete filling material and its application in gob-side entry retaining technology in deep mines. *Buildings* **2024**, *14*, 722. [CrossRef]
20. Manikandan, V.; Jappes, J.W.; Kumar, S.S.; Amuthakkannan, P.J.C.P.B.E. Investigation of the effect of surface modifications on the mechanical properties of basalt fibre reinforced polymer composites. *Compos. Part B Eng.* **2012**, *43*, 812–818. [CrossRef]
21. Chen, H.; Xie, C.; Fu, C.; Liu, J.; Wei, X.; Wu, D. Orthogonal analysis on mechanical properties of basalt-polypropylene fiber mortar. *Materials* **2020**, *13*, 2937. [CrossRef] [PubMed]
22. Zhang, X.; Lou, C.; Lyu, X. Experimental study on direct tensile fatigue performance of basalt fiber reinforced concrete. *Sci. Rep.* **2024**, *14*, 765. [CrossRef] [PubMed]
23. Nguyen, N.T.; Bui, T.T.; Bui, Q.B. Fiber reinforced concrete for slabs without steel rebar reinforcement: Assessing the feasibility for 3D-printed individual houses. *Case Stud. Constr. Mater.* **2022**, *16*, e00950. [CrossRef]
24. Dong, H. Preparation and performance analysis of polypropylene fiber-reinforced concrete composite. *Asia-Pac. J. Chem. Eng.* **2020**, *15*, e2445. [CrossRef]
25. Islam, M.S.; Church, J.S.; Miao, M. Effect of removing polypropylene fibre surface finishes on mechanical performance of kenaf/polypropylene composites. *Compos. Part A Appl. Sci. Manuf.* **2011**, *42*, 1687–1693. [CrossRef]
26. Liu, Y.; Wang, L.; Cao, K.; Sun, L. Review on the durability of polypropylene fibre-reinforced concrete. *Adv. Civ. Eng.* **2021**, *2021*, 6652077. [CrossRef]
27. Suksiripattanapong, C.; Phetprapai, T.; Singsang, W.; Phetchuay, C.; Thumrongvut, J.; Tabyang, W. Utilization of recycled plastic waste in fiber reinforced concrete for eco-friendly footpath and pavement applications. *Sustainability* **2022**, *14*, 6839. [CrossRef]
28. Kumar, S.; Doshi, H.; Srinivasarao, M.; Park, J.O.; Schiraldi, D.A. Fibers from polypropylene/nano carbon fiber composites. *Polymer* **2002**, *43*, 1701–1703. [CrossRef]

29. Xu, J.; Li, H.; Huang, S.; Pi, Z.; Chen, J.; Chen, X.; Song, J. Comparative study on the properties of basalt and steel fiber reinforcement waste rock concrete. *Sci. Rep.* **2025**, *15*, 15103. [CrossRef]
30. *GB/T 50081-2019*; Standard for Test Methods of Concrete Physical and Mechanical Properties. China Architecture & Building Press: Beijing, China, 2019.

Disclaimer/Publisher's Note: The statements, opinions and data contained in all publications are solely those of the individual author(s) and contributor(s) and not of MDPI and/or the editor(s). MDPI and/or the editor(s) disclaim responsibility for any injury to people or property resulting from any ideas, methods, instructions or products referred to in the content.